Universal Nanopore Platform Integrating Multiple Resistive Pulse Sensors into a Single Microfluidic Device

Marcus Pollard,[1] Rushabh Maugi,[1] Angelika Holzinger,[2] Micheál D. Scanlon,[2] Mark Platt[1*]

1 – School of Science, Loughborough University. Epinal Way. LE11 3TU

2 - The Bernal Institute and Department of Chemical Sciences, School of Natural Sciences, University of Limerick (UL), Limerick V94 T9PX, Ireland

* Corresponding author m.platt@lboro.ac.uk

Abstract

Resistive pulse sensors have been used to characterise everything from whole cells to small molecules. Their integration into microfluidic devices have simplified sample handling whilst increasing throughput. Typically, these devices measure a limited size range or a specific analyte, making them prone to blockages in complex sample matrixes. To prolong their life and facilitate their use, samples are often filtered or prepared to match the sample with the sensor diameter. Here, we advance our tuneable flow resistive pulse sensor which utilises additively manufactured parts. The sensor allows parts to be easily changed, washed and cleaned, its simplicity and versatility allows components from existing nanopore fabrication techniques such as silicon nitride, polyurethane and glass pipettes to be integrated into a single device. This creates a multi-nanopore sensor that can simultaneously measure particles from 0.1 to 30 μm in diameter. The orientation and controlled fluid flow in the device allows the sensors to be placed in series, whereby smaller particles can be measured in the presence of larger ones without the risk of being blocked. We demonstrate the device with a range of nanopore materials commonly found within the literature, the easiest to set up was the pulled glass pipette and glass nanopore membrane. However, the glass nanopore membrane was by far the most robust and reusable component tested. We illustrate the concept of a multi-pore flow resistive pulse sensor, by combining an additively manufactured tuneable sensor, termed sensor 1, with a fixed nanopore sensor, termed sensor 2. Sensor 1 measures particles 2 to 30 μm in diameter, whilst sensor 2 can be used to characterise particles as small as 100 nm, depending upon its dimensions.

Keywords: Resistive Pulse Sensor, Nanopore, Additive Manufacturing, Microfluidic

Introduction

From its early applications of cell counting in the 1950's, the Coulter Counter technology continues to be advanced and improved. Increasingly known as resistive pulse sensing/ sensors (RPS), devices based on this principle have now been created from a range of materials from graphene,[1–3] to polymers,[4,5] silicon nitride[6] and glass.[7–11] The sensing process is simple, by monitoring the temporary changes in current caused by the translocation of an analyte through a narrow constriction, termed a sensing region or pore, RPS can characterise analytes according to size,[12] concentration,[13] shape[14–17] and charge.[18] The transport of an analyte through the pore is controlled by tuning the applied electric field, charge on the pore wall, electrophoretic mobility of the analyte, supporting electrolyte concentration and induced convection.[19,20] To maintain sensitivity the pore size must be of comparable dimensions as the analyte.[5] Therefore, whilst a smaller sensing region can detect smaller analytes, the drawback is an increases the likelihood of blockages, and a decreased translocation frequency.

Recent advances in the RPS sensors have utilised pores of different aspect ratios/shapes or specific electrode configurations to allow utilise larger pores and sensing zones.[21–24] When integrated into microfluidic systems this technology is further advanced,[25–29] allowing users to combine sample handling within the analytical system. A variety of innovations in this area, summarised in reviews elsewhere,[30,31] have focused on different forms of fabrication, convection and applications. For example, electrophoresis can be used to drive the analyte through the pore. One example uses an applied electric field of 60 V to drive the sample flow for the detection of bacteria.[32] Similar designs have coupled syringe pumps with lower voltages for the detection of yeast cells,[28] polystyrene particles[21,33], DNA[33], red blood cells[25] and algae.[34] Another advantage of controlling convection and the design of the sensing zone is the ability to force the analyte through a series of RPS sensing regions. Zhang *et al*.[25] presented such a device where five identical sensing regions were arranged in series. As the analyte travelled through the device it generated five pulses, allowing each analyte to be measured multiple times, whilst providing a regular signal pattern to be identified against random background fluctuations. The authors suggest that such a device could improve the signal-to-noise ratio by a factor of $n^{1/2}$, where n is the number of sensing regions.

An emerging fabrication process for microfluidic systems is additive manufacturing (AM) or 3D printing.[35–37] In the field of microfluidics the use of 3D printing and lab-on-a-chip fabrication has increased.[35,37–39] Examples of RPS components integrated into AM are limited. This is likely due to the print resolution, although the use of two-photon-polymerisation (2PP) has now enabled some novel nanopore designs.[40] We have previously used surface channels within AM devices, sealed with a polymer acetate film to overcome the resolution of AM.[41] In a subsequent design, we extended the sensing dynamic range down to 5 μm using a re-sealable lid

and tuneable PDMS gasket layer.[15] However, this was insufficient to study nanomaterials.

To show how an AM-RPS device can be improved to cover a wide particle size range, here we present a beyond-state-of-the-art AM-RPS sensor design with advanced functionality by creating a system of fully integrated AM components. The motivation behind this work was to extend the detection range of the device, whilst making it easier to fabricate, reuse and be less prone to blockages. The final device creates a series of RPS sensors that can be independently tuned to an analyte size range of interest. We combine the additively manufactured tuneable sensor, termed sensor 1, with a fixed nanopore sensor, termed sensor 2 (see figure 1). The only restriction in design criteria is that sensor 1 must be tuned to a size range equal to or larger then sensor 2. We adhere to this restriction by using Sensor 1 to measure particles 2-30 μm in size, whilst sensor 2 characterises particles as small as 100 nm. In the configurations shown in figure 1, the liquid always flows through sensor 1 and then, depending upon the setup, either flows over the surface of sensor 2 (figure 1ai) or through and around sensor 2 (figure 1aii). For nanomaterials to enter sensor 2, they must traverse the opening *via* a combination of electrophoresis (EP), osmosis (EO) or convection (figure 1b). These novel configurations facilitate the measurement of the broadest size range to date on a single device and represent the first integration of solid state nanopores into an AM-RPS. Critically, the orientation and controlled fluid flow in the device allows the sensors to be placed in series, whereby smaller particles can be measured in the presence or larger ones without the risk of the pores being blocked.

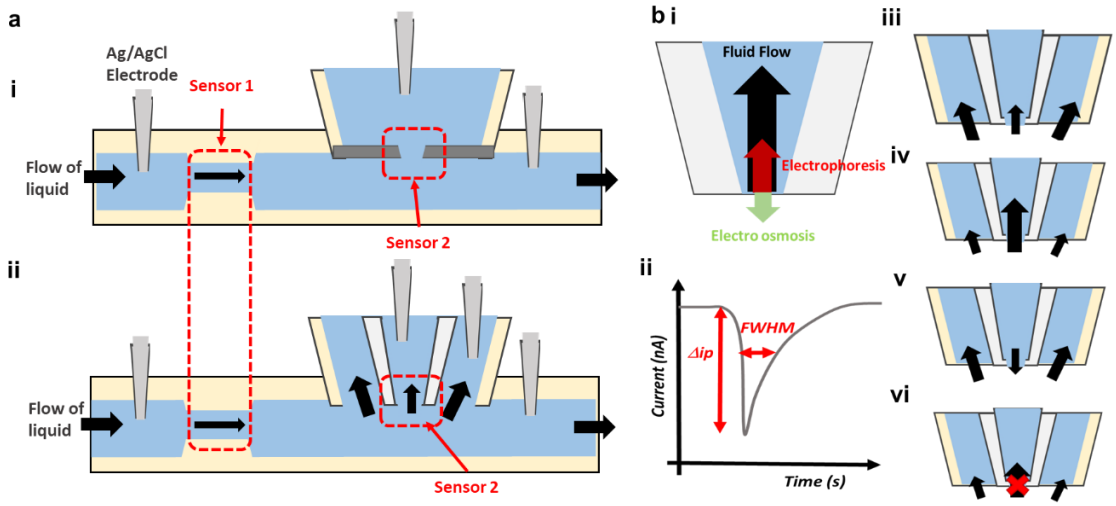

Figure 1. *a) Schematic of the dual pore setup showing the location of the sensors, electrodes and fluid flow for silicon nitride (SiN), silicon dioxide (SiO_2) and polyurethane (PU) pores (i) and glass pipettes and glass nanopore membranes (GNMs) (ii). b) i) Illustration of the forces acting upon the particles through sensor 2, ii) Schematic of a blockade event or pulse in sensor 1 and 2, the pulse depth Δ_{ip} is proportional the to the analyte volume, and the full width half maximum (FWHM) the speed of the analyte through the sensing zone. The black arrows in iii-vi represent fluid flow, where by controlling the flow ratios the flow through sensor 2 can be stopped (vi).*

Experimental Methods

Chemicals and materials. Particles 100nm – 2 μm were obtained from Izon Science Ltd, CPC100 (mean diameter 110nm), CPC200 (mean diameter 200nm) CPC2000, 2 micron carboxylated polystyrene calibration particles, 10 micron and 20 micron carboxlyated polystyrene calibration particles denoted as CP10M and CP20M were obtained from Izon Science Ltd. 30 μm carboxylated polystyrene particles, Cat No. 84135, ethanol >99.8 %, acetone >97%, sulphuric acid 95-97% and 30% (w/w) perchloric acid were obtained from Sigma-Aldrich, potassium chloride obtained from Fisher Scientific UK, >99% cat no: P/4240/60, Acc Silicones QSil216 was obtained from RS components, catalogue no: 458-765, part no: QSil 216. Lambda DNA (λ-DNA 10745782001) were obtained from Fisher Scientific. The λ-DNA was used as received or diluted to the required solution. Silicon (SiN, SiO_2) membranes, and custom faraday cages were purchased from Nanopore Solutions (nanoporesolutions.com), glass nanopore membranes (GNMs) from Electronic BioSciences USA and glass pipettes from World Precision Instruments (WPI) Europe. Silver wire >99.9% cat AG5487 was obtained from advent-rm. Fluid cell holders we designed and printed from SLA resin and supplied through SGD printing services. Data analysis was performed within the data analysis module of the Izon control suite. Pulse shape extraction as performed using molecular devices clampfit version 10.7. Dolomite mitos-P Pumps were used to supply the flow, current amplifiers were supplied from Elements-ic, or were removed and repurposed from a Izon Qnano system for sensor 2. Sampling frequencies were 50-60kHz with a 5 kHz bandpass filter. Flow rates were monitored by collecting the liquid from the outlets and weighing the solution over a period of time.

Dielectric breakdown set-up. A silicon membrane, either SiN or SiO_2, was mounted into a holder (nanoporesolutions.com) and washed with 1 M KCl solution. Two electrodes were then inserted into each of the fluid cells, with one connected to a power source consisting of either a DC regulated power supply (obtained from Circuit Specialists) or a bank of 1.6 V batteries. The power supply was also connected to a multimeter (FLUKE 179), which was in turn connected to the remaining electrode in the pore holder.

Development of a wetting method. The pores were initially cleaned post fabrication to remove any contaminants by submerging them in piranha solution (3:1 mixture of H_2SO_4 and 30% (w/w) H_2O_2 for 5 min., followed by their submersion in deionised water. The pores were then cleaned in an acetone bath and the process repeated with ethanol to remove any residual contaminants. Also, ethanol's low surface tension aids the removal of air bubbles. Next, the pores were plasma treated in air for 30 s per side and then loaded into the measurement cell, where they were wetted with a small amount of ethanol (approximately 25-50 μL). The ethanol was replaced with buffer until the baseline current was stable.

Nano- and micropores fabricated *via* focused ion beam (FIB) milling. Single pore SiN membranes with varying pore diameters were fabricated *via* FIB milling (30 kV, 7.7 - 24 nA) with a focused ion beam/scanning electron microscope (FIB/SEM) dual beam system (Ga ion beam, Helios G4 CX DualBeam, ThermoFisher Scientific).

Pore imprinted polymer (PIPS) method. A section of thermoplastic polyurethane (PU; Delstar EU40, 36 μm in thickness, obtained from SWM) was mounted onto a sheet of aluminium foil. The membrane was then placed on top of a hotplate and a weighed tungsten needle (from Agar Scientific) positioned on top of the membrane. A temperature of 50^{o}C softened the membrane sufficiently to pierce with the tungsten needle without changing the membrane's physical characteristics. A higher temperature of 55^{o}C caused the membrane to discolour, with bubbles beginning to form. At 60^{o}C, the membrane became very malleable and was too difficult to handle. Two methods were evaluated to prepare the pores. The first was the aforementioned approach, where a weighted needle was placed on top of the membrane during the heating process. The second investigated if the pores would shrink or reseal upon heating. This involved heating a previously prepared pore back to the fabrication temperature, with the pore's size and shape recorded before and after heating.

Device assembly. In order to assemble the device, the lid was either affixed to the base *via* 6 machine screws or using a clip (figures 2 and S1). HPLC fittings were inserted into each screw thread to accommodate the inlet from the pumps, electrodes and the outlet. Once fully assembled, the device was placed into a custom-made Faraday cage and electrolyte solution was pumped into the device. The PDMS was poured onto side of the lid with the ridge, such that the PDMS covered the entire lid surface and was <1mm in thickness.

Device Printing. The lid, screw threads and base of the device were printed using an Asiga Pico HD27 UV 3D printer with FORMlabs clear resin. Design files were converted from the CAD software (Siemens NX11) to STL and prepared for printing using Asiga Composer software. Once printed, the parts were cleaned and post cured using a UV light box more details

Polydimethylsiloxane (PDMS) gasket. The PDMS gaskets were formed by mixing parts A and B of QSil 216 clear liquid silicone in a 10:1 ratio. The lid was placed into a petri dish with the ridge oriented to the bottom. The uncured PDMS was then poured around the edge of the lid making sure that the whole lid was covered up the ridge and no air pockets remained. The PDMS was then cured for 1 hr at 70^{o}C or until set.

Optical Imaging. Microscope images were captured using a Nixon Optiphot 2 optical microscope and optical images were captured using a DS 5M camera with a DS-L1 camera control unit.

Electrode fabrication. Electrodes were fabricated by inserting a section of 0.25 mm diameter silver wire (99.99% purity, Advent Research Materials) into a pipette

tip. A small section of the wire was threaded through the narrow end of the pipette, glued in place using Araldite® Rapid epoxy resin and then left to dry.

Results and Discussion

The concept involves using our previously published AM tuneable flow device[15] as a core, referred to here as the “fluidic chip”. Exploiting the fluidic chip as the central part to build upon allowed other electrodes and RPS sensors to be added (figure 2). To facilitate ease of use, a custom holder for the device was created replacing the 6 screws that previously held the lid and base together, as shown in figures 2biii and S1.

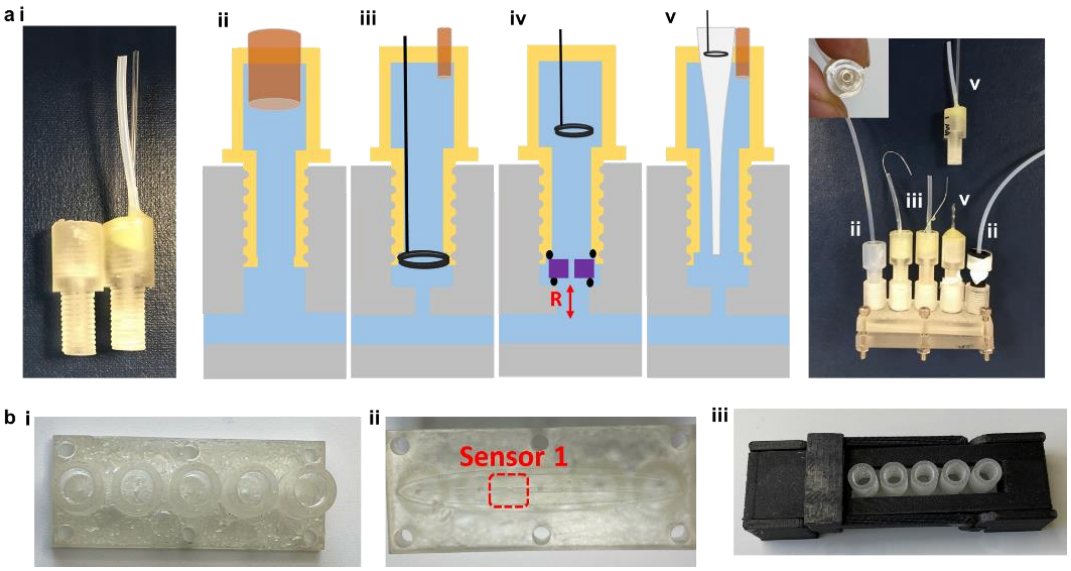

Figure 2. *a) The HPLC screw thread and mounted glass pipette and exit tube (i). Schematic of the different components – Inlet/outlet (ii), Ag/AgCl reference electrode (iii), SiO_2, SiN and PU holder with the recess illustrated as R (iv), and glass pipette and GNM holder with exit tube (v). Illustrative example of all components in an assembled device. b) Example base unit with screw ports (i), reverse side of base unit showing sensor 1 (ii), and with an assembled device and holder (iii).*

Sensor 1. The base and lid had the same design as reported previously.[15] Briefly, the fluidic chip was made of a base unit and lid, that when placed together created a RPS sensing zone, termed sensor 1. The base contained a surface channel and using this method, commercial stereolithography (SLA) printers and resins reproducibility produce channels ≥ 100 μm.[41,42] The lid had a ridge that matched the shape and dimensions of the channel and extended 1 mm out from the lids surface. Optical images of the channel are shown in figure 2bii. A PDMS gasket between the lid and base sealed the components preventing any leakage. The PDMS layer was typically 1mm in thickness and when placed between the lid and base acted as a spacer to prevent the ridge entering the channel. The shape or dimensions (internal volume) of the sensing zone were controlled by compressing the PDMS layer, forcing the ridge on the lid deeper into the channel (figure S1c).[15] Changing the volume of the sensing

zones allowed the sensitivity of the RPS sensor to be tuned. The tuneability of sensor 1 was controlled by turning a single screw on the back of the holder, which in turn increased the force on the lid (figure s1c). Upon tightening the screw in the back of the holder, the blockage magnitude of the same sized particles increased. Thus, a device printed with initial channel dimensions of 100×100×500 μm can measure particles from 2 to 30 μm in diameter (see figure S2).

For simplicity, the Ag/AgCl reference electrodes were incorporated into a HPLC style and sized, screw thread (figure 2a). Alongside the Ag wire, a tube was inserted into the screw thread to allow any trapped air bubbles to be removed during filling, and was usually sealed during operation, *i.e.,* no flow was observed out of the reference electrode port during sensing. To simplify the number of parts and designs, the same sized screw thread was used to insert other parts and components. As shown in figure 2 (top right image), the screw thread was used for the inlet, outlets, reference electrodes and subsequent RPS materials.

Sensor 2 (materials). To expand the sensing range of the device to particles smaller than 2 μm, an additional RPS sensor was needed, termed sensor 2. Within the literature, a range of materials have been tested for RPS applications, and some of the most common solid state materials are SiN and SiO_2. In keeping with our philosophy to create an easy to fabricate and assemble device, we opted to first create pores in SiN or SiO_2 using a dielectric breakdown procedure. Also referred to as controlled dielectric breakdown, this approach was first reported for nanopore fabrication by Kwok *et al.*[43,44] and produces nanopores by applying a potential across a thin membrane (<50 nm). The advantages of dielectric breakdown are the low cost and ease of assembly of the fabrication setup. The technique is commonly used for analysing and sequencing DNA,[45,46] and has also been used to produce arrays within a microfluidic channel.[47]

The process of making and testing the SiN and SiO_2 pores was carried out in a series of stages. Before being placed into the fluidic chip, the membrane holder used to form the pores also allowed the pores to be tested as RPS sensors by placing Ag/AgCl electrodes either side of the membrane connected to a current amplifier to the setup. Thus, to confirm pore formation, the translocation of λ-DNA through the pore was measured (figure s3). Upon detection of λ-DNA, the pore was enlarged under an applied electric field[44,47] to allow further detection of nanomaterials (Figure s3). Once the pore had been enlarged it could be used to measure the translocation events of nanoparticles, an example of which is shown in figure 3a. The successfully fabricated pores were able to detect different sized particles, however they were limited < 5 runs each pore, and subsequent washing with buffer and ethanol could not restore translocation events. Not all the pores survived, as the enlarging process caused the pores to become brittle, crack or produce a baseline noise level that made them unusable (data not shown). The success rate of enlarging pores to sizes capable of detecting nanomaterials > 100nm was 14%. When a suitable pore was found, they were only capable of running a few samples before blocking and attempts to restore

them proved unsuccessful, thus they were not able to be transferred into the fluidic chip.

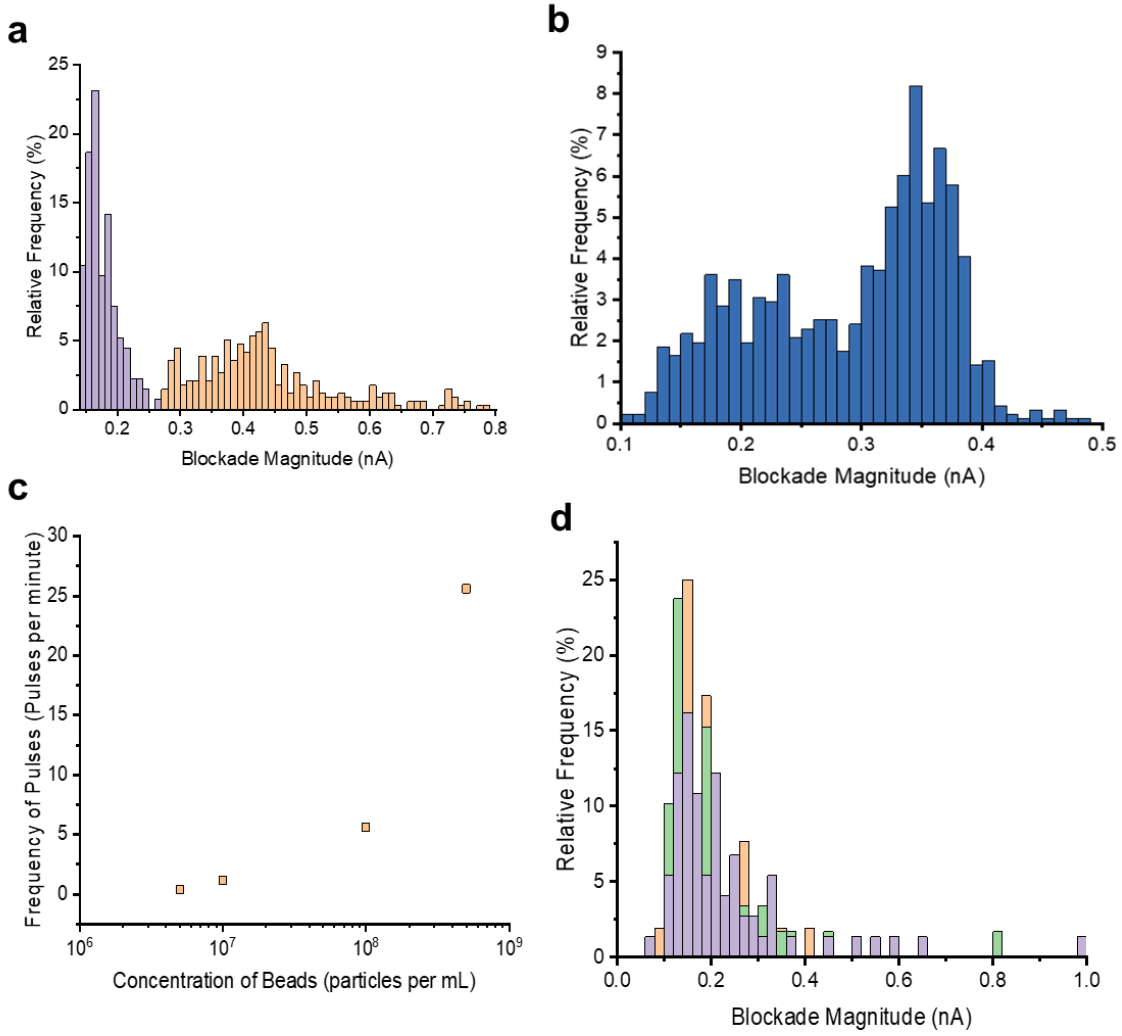

Figure 3. *a) Dielectric breakdown SiN pore. Histogram for 110 nm particles (purple) and 150 nm (orange) particles, in 50 mM KCl at 1 V, at 2 x 10^9 particles per mL (100 nm) and 9.2 x 10^8 particles per mL (150 nm). b) FIB SiN pore. Histogram of a mixture of 150 nm and 200 nm particles at 0.34 V in 50 mM KCl at a concentration of 7 x10^5 particles per mL c) FIB SiN pore. Particle rate vs. concentration for 200 nm particles, the data was recorded on a 1000 nm pore, at 0.4 V in 50 mM KCl d) PU pore. Histogram for 2000 nm particles recorded at 0.14 V in 10 mM KCl at a concentration of 2.25 x 10^7 particles per mL, the three colours represent three runs on the same pore.*

Whilst easy to setup, the controlled dielectric breakdown process proved to be inconsistent. An alternative fabrication method for SiN and SiO_2 pores is to use a focused ion beam (FIB) to fabricate single nano- or micropores in thin membranes of a desired size from 200 nm to 5 μm (in diameter) as determined by SEM (see figure S4a,b). FIB produced consistently shaped pores regardless of their size. In contrast to the dielectric breakdown method, pores were produced in all of the membranes milled *via* FIB and, as a result, far more pores could progress onto the next stages of testing. However, the pores were found to be difficult to wet, as they had not been created within an electrolyte solution (as was the case with the electric breakdown

setup). Before they were placed into the fluidic chip the FIB-milled pores were first tested in a static liquid cell with nanoparticles to see if translocations could be observed. Figure 3b,c, shows the pulse distribution for two FIB pores and the relationship between pulse frequency and concentration. The success rate of detecting particles with FIB-milled pores prior to their insertion within the fluidic device was circa 45% of the pores that were made, this number may reflect the diameter of the pore and RPS user ability. FIB pores of different diameters and thicknesses may result in different efficiencies.

An alternative approach to nanopore fabrication is to puncture sheets of polyurethane (PU) with needles.[48] Here we attempted a similar process to produce polymer imprinted pores (PIPs) as described in the experimental methods *vide supra*. Examples of pores produced by this method are shown in figures S4c,d. Table S1 summarises the large range in diameters, from 5 to 50 μm, for the PIPs produced. While reproducibly controlling their size and shape was not possible using the current set-up, the PIPs were easily wet with electrolyte solution and data was collected for the detection of particles as small as 2 μm in diameter using 11 μm diameter pores (figure 3d). Thus, with PIPs, pores may be produced easily within a limited set-up but with the trade-off of significantly reduced reproducibility.

Despite the variability of the pore size, the three materials tested here all showed an ability to detect and count nano/micro-materials. A universal mounting system to integrate these into the fluidic chip was then designed. The first iteration of this design is shown in figure 1aiv. The membrane material was sandwiched between two O-rings and held in place within the fluidic chip *via* the standard screw thread. A Ag/AgCl reference electrode was positioned behind the membrane.

Sensor 2 with flow. To test the pore holder within the fluidic chip, an initial assessment of the baseline current was carried out to illustrate the pore was wet and able to conduct a current. A silicon membrane, either SiN or SiO_2, could be placed into the screw thread along with a small amount of ethanol to remove air bubbles from the top and bottom o-rings. Once the pore was wet, the holder was attached to the fluidic device (Figure 1ai) and the ethanol replaced with an electrolyte. A typical baseline current is shown in figure S5. Regardless of flow rate, voltage and particle concentration, no translocations were observed when 400 nm particles flowed into the fluidic device, and this observation was consistent across multiple SiN and SiO_2 pores.

The lack of particle translocations across the SiN and SiO_2 pores was hypothesised to be due to the pores being mounted perpendicular to the main channel and flow. Here, the particles were not pushed into the sensor *via* convection and relied on EP or EO to traverse the pore. This, coupled with the fact the pore was recessed from the main flow by a distance *R* (figure 2), resulted in no particle translocations. It should be noted that the distance *R*, was not explored or optimised in this study, and was estimated to be circa 2 mm in the setup. In the absence of flow, after the main fluid channel was filled with a nanoparticle solution, and the device was left undisturbed for time periods in excess of 30 mins, some particles diffused into the

recess and translocations were observed, but the translocation numbers were inconsistent.

Subsequently, a PU pore was cut out and placed into the screw thread in the same way. The diameter of the PU pore was 50 μm, and 20 μm diameter particles were added to the solution. In the presence of flow through the fluidic chip translocations were observed. A current trace is shown in figures 4a,b. The pulse rate was dependent upon the flow rate, and in the absence of flow, when the fluidic chip was filled with the particles, some translocation events could still be observed (figure 4c). The translocation speed, measured by the pulse width, was much slower in the absence of flow (figures 4b, d). The ability to see translocation in the absence of flow is likely due to the particles settling to the bottom of the device and entering the pores *via* gravity (figure 4e). Given the large size of the particles and pore, the likelihood is that the particles are driven through the pore *via* convection rather than EP. The larger PU pore size allowed the fluid to flow through the pore as well as the outlet of the fluidic chip. This facilitated the translocations observed in the PU sensor 2. As the pore diameter for sensor 2 becomes is reduced i.e. with <1 μm for SiN and SiO_2 pores, the flow of liquid *via* convection through the pore is smaller, favouring the outlet tube in the device. Closing the outlet of the device and forcing the fluid flow through the SiN pores, resulted in the pores breaking/ cracking under the pressure.

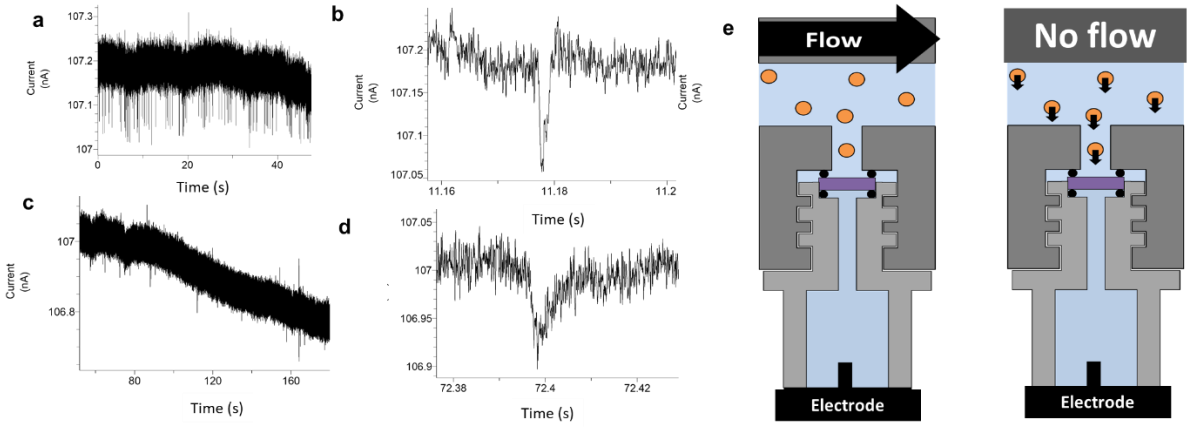

Figure 4. *a) Current trace for 20 μm particles translocating through a 50 μm PU pore, at 0.5 V in 10 mM KCl at a concentration of 7.02 x 10^2 particles per mL, under a pressure of 50 mbar. b) An illustrative pulse from the trace in a. c) Current trace under the same conditions as a), with no flow. d) An illustrative pulse from the trace in c. e) A schematic showing the effect of flow and no flow on the suspended particles*.

An alternative material used in RPS methods is the pulled glass pipette, or glass nanopore membrane, GNM.[49–51] A GNM was mounted into the screw thread shown in figures 2a and 5a, respectively. Alongside the pipettes or GNM's we mounted an alternative exit tube to allow the main liquid flow to exit out of the screw thread next to the pipette RPS sensor. This enabled the samples to be drawn over the glass RPS sensing zone despite the recess from the main channel. The ends of the pipettes and GNM's were also connected to a syringe that allowed liquid to be pulled from the main

fluidic chamber through the RPS material, or *vice versa* (figure 1aiii - vi), a full schematic of the device with its components is shown in figure 5a. Figure 5b shows the particle count rate for a 990 nm diameter GNM sensor 2 with 300 nm diameter particles in the sample liquid. Translocation events were observed instantly as the sample was flowed through the device. Where the flow rate through the main channel increased, the translocation frequency also increased, figure 5b. Halting the flow, resulted in a decrease in translocation events, but did not result in a loss of the signal altogether as the particles can move through the RPS sensors via a combination of EO and EP, grey line figure 5bi. This suggests the device could also be used as an injection loop to measure samples in the absence of flow. The velocity through the GNM, measured by the full width at half maximum (FWHM), also illustrates the effect of the flowing solution. In the absence of a flow, the particles traverse the sensor relatively slowly with a FWHM of 0.5ms, upon the addition of the flow the FWHM decrease to 0.12ms. The velocity does not decrease further as the flow rate goes from 0.5 to 0.75 mL/min. The decrease in FWHM suggests the presence of some additional convection through the pore. The pulse magnitude decreases from 0.26nA to 0.21nA as the flow rate through the main channel increases, the cause for this is not clear, figure 5bii.

As the device works by drawing the sample across the RPS orifice and through the exit tube, akin to the reverse of a flow focusing chamber in flow cytometry, it was hypothesised that alongside the enhanced particle counting rate, the additional flow may help wash/clean and unblock the pore mouth if larger aggregates were present in solution. To test this hypothesis, a GNM was placed into the fluidic chamber, the solution filled with 300 nm particles, and the pulse frequencies were measured (figure 5c). Into this solution, 10 μm particles were also placed at a concentration of 1×10^7 particles/mL. The presence of the larger particles had no effect on ease, speed and consistency of particle translocations (figure 5c). The presence of the larger particle did not inhibit or change the measurement of the smaller ones. The larger 10 um particles could still be counted in the same device simultaneously using sensor 1. This ability to measure a wide range of particle sizes, or the properties of smaller ones without the need for sample preparation and filtration, may have many applications in biological and physical sciences.

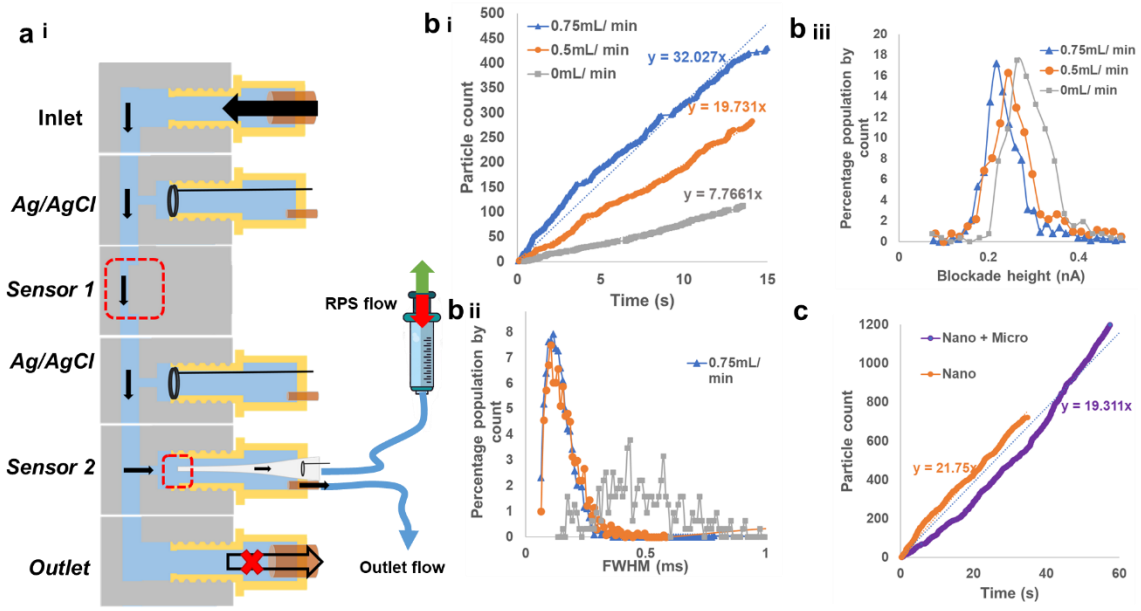

Figure 5. *a) Schematic of the fluid chip and its components, connected to the outlet of sensor 2 was a syringe, where flow through the GNM could be enhanced (PLUS) or inhibited. b) 990 nm GNM sensor 2 using 300nm diameter particles, 1 x 10^9 particles/ mL. 1.68V. Flow rates are measured at the outlet of sensor 2. i) Translocation frequency. ii) Blockade magnitude histograms, iii) FWHM values. c) Translocation frequency of using 300nm diameter particles through a 990 nm GNM sensor 2, 1 x 10^9 particles/ mL. 1.68V in the absence (Nano) and presence (Nano +Micro) of 10 μm particles 1 x 10^7 particles /mL.*

In theory, the addition of a syringe to the back of sensor 2 allows the user to increase the fluid flow through the GNM, by pulling the syringe out, or prevent the convection through the pore by pushing the syringe down. The flow rate through the centre of the pipette was difficult to measure, given its small volume, and the flow rate ratios are not known here. It may be possible to control this further in more advanced systems and is the focus of future work. However as the ratio of flow was changed to allow more liquid through the GMN i.e. the syringe was pulled to draw liquid through the sensor, the pulse frequency also increased (figure 6). Conversely, when the liquid flow was reversed back from the GNM into the main channel, no translocation events were observed (no data available to plot in figure 6) as a comparison the blockade size, frequency and translocation speed of the particles in the absence of any additional flow from the syringe is also shown in figure 6.

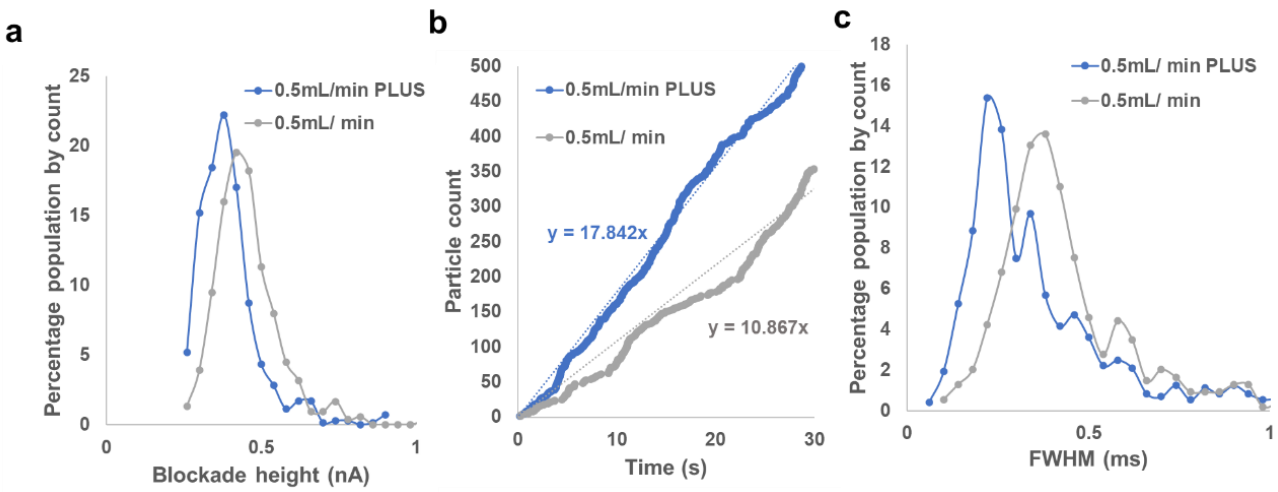

Figure 6. *a) Distribution of blockade height and b) Translocation frequencies, c) FWHM values using a 780 nm pore size in a GNM, 1.9V in 50 mM KCl and a particle concentration of 200 nm particles 1 x 10^9 particles/ mL. To create a PLUS liquid flow through the RPS a Syringe was withdrawn to value of 3mL and held in a fixed position until after the experiments. To inhibit the flow through the RPS a syringe was depressed by a value of 1 mL.*

Conclusions

In this article, we create a tuneable flow resistive pulse sensor which utilises additively manufactured parts. The sensor allows parts to be easily changed, washed and cleaned, its simplicity and versatility allows components from existing nanopore fabrication techniques using SiN, SiO_2, or polyurethane membranes and glass pipettes to be integrated into a single device. This creates a multi-nanopore sensor that can simultaneously measure particles from 0.1 to 30 μm in diameter. The orientation and controlled fluid flow in the device allows the sensors to be placed in series, whereby smaller 200 nm particles can be measured in the presence of 10 μm particles without the risk of being blocked. Upon testing the device, SiN and SiO_2 pores were found to have a low reproducibility. The most reproducible sensor material was the pulled glass pipette. Using GNM's further enhanced the ease of the device was they were robust and could be easily cleaned *via* sonication and reused. This allowed the same GNM to be used many times. The device here could greatly enhance the detection of microorganisms, characterise biological and inorganic nanomaterials with little or no sample preparation, and offers a platform that can be added to or run in series with other RPS fluidic chips or complimentary analytical technologies.

Supporting Information Available

Supporting Information Available:

References

1 S. Nam, I. Choi, C. Fu, K. Kim, S. Hong, Y. Choi, A. Zettl and L. P. Lee, *Nano Lett.*, 2014, **14**, 5584–5589.

2 R. R. Henriquez, T. Ito, L. Sun and R. M. Crooks, *Analyst*, 2004, **129**, 478–482.

3 T. Ito, L. Sun, R. R. Henriquez and R. M. Crooks, *Acc. Chem. Res.*, 2004, **37**, 937–945.

4 G. S. Roberts, D. Kozak, W. Anderson, M. F. Broom, R. Vogel and M. Trau, *Small*, 2010, **6**, 2653–2658.

5 E. Blundell, L. J. Mayne, E. R. Billinge and M. Platt, *Anal. Methods*, 2015, **7**, 7055–7066.

6 J. B. Heng, A. Aksimentiev, C. Ho, P. Marks, Y. V Grinkova, S. Sligar, K. Schulten and G. Timp, *Biophys. J.*, 2006, **90**, 1098–1106.

7 W.-J. Lan, D. A. Holden, J. Liu and H. S. White, *J. Phys. Chem. C*, 2011, **115**, 18445–18452.

8 M. Lemmer, M. S. Inkpen, K. Kornysheva, N. J. Long and T. Albrecht, *Nat. Commun.*, 2016, **7**, 12922.

9 G. Nguyen, S. Howorka and Z. S. Siwy, *J. Membr. Biol.*, 2011, **239**, 105–113.

10 H. S. White and A. Bund, *Langmuir*, 2008, **24**, 2212–2218.

11 W.-J. J. Lan, C. Kubeil, J.-W. W. Xiong, A. Bund and H. S. White, *J. Phys. Chem. C*, 2014, **118**, 2726–2734.

12 C. Bernabini, D. Holmes and H. Morgan, *Lab Chip*, 2011, **11**, 407–412.

13 A. D. Grabarek, D. Weinbuch, W. Jiskoot and A. Hawe, *J. Pharm. Sci.*, 2019, **108**, 563–573.

14 R. Maugi, P. Hauer, J. Bowen, E. Ashman, E. Hunsicker and M. Platt, *Nanoscale*, 2020, **12**, 262–270.

15 M. Pollard, E. Hunsicker and M. Platt, *ACS Sensors*, 2020, **5**, 2578–2586.

16 C. Chan, W. Mak, K. Cheung, K. Sin, C. Yu, T. Rainer and R. Renneberg, *Annu. Rev. Anal. Chem.*, 2013, **6**, 191–211.

17 N. A. W. Bell and U. F. Keyser, *Nat Nano*, 2016, **11**, 645–651.

18 E. L. C. J. Blundell, R. Vogel and M. Platt, *Langmuir*, 2016, **32**, 1082–1090.

19 L. Mayne, C. Y. Lin, S. D. R. Christie, Z. S. Siwy and M. Platt, *ACS Nano*, 2018, **12**, 4844–4852.

20 R. Vogel, G. Willmott, D. Kozak, G. S. Roberts, W. Anderson, L. Groenewegen, B. Glossop, A. Barnett, A. Turner and M. Trau, *Anal. Chem.*, 2011, **83**, 3499–3506.

21 R. Peng and D. Li, *Talanta*, 2018, **184**, 418–428.

22 H. Yasaki, T. Yasui, T. Yanagida, N. Kaji, M. Kanai, K. Nagashima, T. Kawai and Y. Baba, *J. Am. Chem. Soc.*, 2017, **139**, 14137–14142.

23 P. Hinkle, T. M. Westerhof, Y. Qiu, D. J. Mallin, M. L. Wallace, E. L. Nelson, P. Taborek and Z. S. Siwy, *Sci. Rep.*, 2017, **7**, 10173.

24 Z. Siwy, P. Apel, D. Dobrev, R. Neumann, R. Spohr, C. Trautmann and K. Voss, *Nucl. Instruments Methods Phys. Res. Sect. B Beam Interact. with Mater. Atoms*, 2003, **208**, 143–148.

25 W. Zhang, Y. Hu, G. Choi, S. Liang, M. Liu and W. Guan, *Sensors Actuators B Chem.*, 2019, **296**, 126615.

26 Z. Song, M. Li, B. Li, Y. Yan and Y. Song, *Electrophoresis*, 2019, **40**, 897–905.

27 T. Zhou, Y. Song, Y. Yuan and D. Li, *Anal. Chim. Acta*, 2019, **1052**, 113–123.

28 J. Sun, Y. Kang, E. M. Boczko and X. Jiang, *Electroanalysis*, 2013, **25**, 1023–1028.

29 N. Khodaparastasgarabad, A. Mohebbi and C. Falamaki, *Microsyst. Technol.*, 2019, **25**, 3643–3653.

30 Z. Liu, J. Li, J. Yang, Y. Song, X. Pan and D. Li, *Microfluid. Nanofluidics*, 2017, **21**, 4.

31 Y. Song, J. Zhang and D. Li, *Micromachines*, 2017, **8**, 204.

32 Y. Song, H. Zhang, C. H. Chon, S. Chen, X. Pan and D. Li, *Anal. Chim. Acta*, 2010, **681**, 82–86.

33 R. Peng and D. Li, *Nanoscale*, 2017, **9**, 5964–5974.

34 Y. Song, J. Wang, J. Yang, Y. Wu, N. Li, N. Gong, X. Pan, Y. Sun and D. Li, *Instrum. Sci. Technol.*, 2012, **40**, 305–315.

35 T. Monaghan, M. J. Harding, R. A. Harris, R. J. Friel and S. D. R. Christie, *Lab Chip*, 2016, **16**, 3362–3373.

36 A. J. Capel, S. Edmondson, S. D. R. Christie, R. D. Goodridge, R. J. Bibb and M. Thurstans, *Lab Chip*, 2013, **13**, 4583–4590.

37 A. J. Capel, R. P. Rimington, M. P. Lewis and S. D. R. Christie, *Nat. Rev.*

Chem., 2018, **2**, 422–436.

38 S. D. R. Capel, A. J.; Wright, A.; Harding, M. J.; Weaver, G. W.; Li, Y.; Harris, R. A.; Edmondson, S.; Goodridge, R. D.; Christie, *Beilstein J. Org. Chem.*, 2017, **13**, 111–119.

39 O. Okafor, A. Weilhard, J. A. Fernandes, E. Karjalainen, R. Goodridge and V. Sans, *React. Chem. Eng.*, 2017, **2**, 129–136.

40 C. Liao, W. Anderson, F. Antaw and M. Trau, *ACS Omega*, 2019, **4**, 1401–1409.

41 S. M. Hampson, M. Pollard, P. Hauer, H. Salway, S. D. R. Christie and M. Platt, *Anal. Chem.*, 2019, **91**, 2947–2954.

42 S. M. Hampson, W. Rowe, S. D. R. Christie and M. Platt, *Sensors Actuators B Chem.*, 2018, **256**, 1030–1037.

43 H. Kwok, K. Briggs and V. Tabard-Cossa, *PLoS One*, 2014, **9**, e92880.

44 K. Briggs, M. Charron, H. Kwok, T. Le, S. Chahal, J. Bustamante, M. Waugh and V. Tabard-Cossa, *Nanotechnology*, 2015, **26**, 084004.

45 C. E. Arcadia, C. C. Reyes and J. K. Rosenstein, *ACS Nano*, 2017, **11**, 4907–4915.

46 I. Yanagi, K. Fujisaki, H. Hamamura and K. Takeda, *J. Appl. Phys.*, 2017, **121**, 045301.

47 R. Tahvildari, E. Beamish, V. Tabard-Cossa and M. Godin, *Lab Chip*, 2015, **15**, 1407–1411.

48 S. J. Sowerby, M. F. Broom and G. B. Petersen, *Sensors Actuators B Chem.*, 2007, **123**, 325–330.

49 S. R. German, L. Luo, H. S. White and T. L. Mega, *J. Phys. Chem. C*, 2013, **117**, 703–711.

50 W.-J. Lan and H. S. White, *ACS Nano*, 2012, **6**, 1757–1765.

51 Y. Zhang, M. A. Edwards, S. R. German and H. S. White, *J. Phys. Chem. C*, 2016, **120**, 20781–20788.

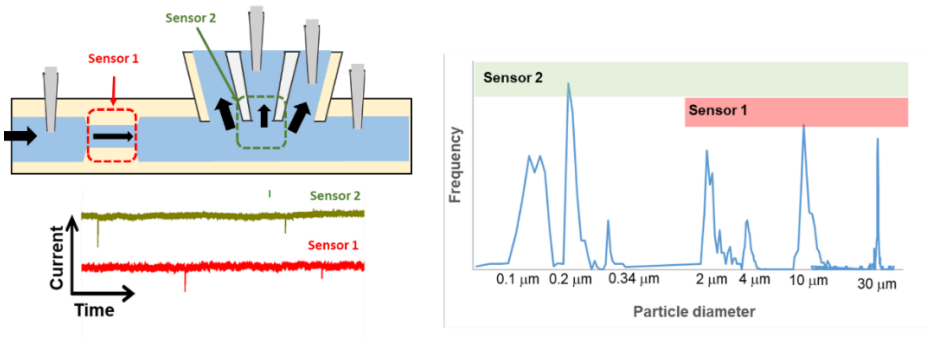
Sensor 2
Sensor 1
Sensor 2
Sensor 1
Current
Time
Sensor 2
Sensor 1
Frequency
0.1 μm
0.2 μm
0.34 μm
2 μm
4 μm
10 μm
30 μm
Particle diameter

TOC image